

Global Datasets of Leaf Photosynthetic Capacity for Ecological and Earth System Research

Jing M. Chen^{1,2}, Rong Wang^{1,2}, Yihong Liu^{2,4}, Liming He³, Holly Croft⁴, Xiangzhong Luo⁵, Han Wang⁶,
5 Nicholas G. Smith⁷, Trevor F. Keenan^{8,9}, I. Colin Prentice^{6,10,11}, Yongguang Zhang¹², Weimin Ju¹², and
Ning Dong^{10,11}

¹~~School of Geography, Fujian Normal University, Department of Geography and Planning, University of Toronto,~~

²~~Department of Geography and Planning, University of Toronto, School of Geography, Fujian Normal University,~~

³Canada Centre for Remote Sensing, Natural Resources Canada,

10 ⁴School of Biosciences, University of Sheffield, Sheffield, UK,

⁵Department of Geography, National University of Singapore

⁶Department of Earth System Science, Tsinghua University, Beijing 100084, China,

⁷Department of Biological Sciences, Texas Tech University, Lubbock, TX, USA

⁸Climate and Ecosystem Sciences Division, Lawrence Berkeley National Laboratory, Berkeley, CA, USA

15 ⁹Department of Environmental Science, Policy and Management, UC Berkeley, Berkeley, CA, USA

¹⁰Department of Life Sciences, Imperial College London, Silwood Park Campus, Buckhurst Road, Ascot SL5 7PY, UK

¹¹Department of Biological Sciences, Macquarie University, North Ryde, NSW 2109, Australia

¹²International Institute of Earth System Science, Nanjing University, China

Correspondence to: Jing M. Chen (jing.chen@utoronto.ca)

20 **Abstract.** The maximum rate of Rubisco carboxylation (V_{cmax}) determines leaf photosynthetic capacity and is a key
parameter for estimating the terrestrial carbon cycle, but its spatial information is lacking, hindering global ecological
research. Here, we convert leaf chlorophyll content (LCC) retrieved from satellite data to V_{cmax} , based on plants' optimal
distribution of nitrogen between light harvesting and carboxylation pathways. We also derive V_{cmax} from satellite (GOME-2)
observations of sun-induced chlorophyll fluorescence (SIF) as a proxy of leaf photosynthesis using a data assimilation
25 technique. These two independent global V_{cmax} products agree well ($r^2=0.79$, RMSE=15.46 $\mu\text{mol m}^{-2}\text{s}^{-1}$, $P<0.001$) and
compare well with 3672 ground-based measurements ($r^2=0.68$, RMSE=13.55 $\mu\text{mol m}^{-2}\text{s}^{-1}$ and $P<0.001$ for SIF; $r^2=0.55$,
RMSE=17.55 $\mu\text{mol m}^{-2}\text{s}^{-1}$ and $P<0.001$ for LCC). The LCC-derived V_{cmax} product is also used to constrain the retrieval of
 V_{cmax} from TROPOMI SIF data to produce an optimized V_{cmax} product using both SIF and LCC information.~~Through a data~~
~~assimilation technique, these two types of V_{cmax} products from remote sensing are combined to provide an optimized V_{cmax}~~
30 ~~product~~. The global distributions of these products are compatible with V_{cmax} computed from an ecological optimality theory
using meteorological variables, but importantly reveal additional information on the influence of land cover, irrigation, soil
pH and leaf nitrogen on leaf photosynthetic capacity. These satellite-based approaches and spatial V_{cmax} products are primed
to play a major role in global ecosystem research. The three remote sensing V_{cmax} products based on SIF, LCC and SIF+LCC

are available at <https://doi.org/10.5281/zenodo.6466968> (Chen et al., 2020) and the code for implementing the ecological
35 optimality theory is available at https://github.com/SmithEcophysLab/optimal_vcmax_R (Smith, 2020).

1 Introduction

The Farquhar-von Caemmerer-Berry (FvCB) leaf photochemistry model (Farquhar et al., 1980) is widely used for simulating
vegetation photosynthesis in ecological studies. The maximum carboxylation rate (V_{cmax}) that determines leaf photosynthetic
capacity is an essential parameter in the FvCB model. The current state of the art (Rogers 2014, Rogers et al., 2017) in
40 regional and global ecosystem modeling is to assign V_{cmax} at 25°C ($V_{\text{cmax}25}$) as a fixed parameter that varies by plant
functional type (PFT), and is typically estimated from a ground-based database (Kattge et al., 2009 and 2020), even though
observations show 2-3-fold variation in $V_{\text{cmax}25}$ for the same PFT. As the total simulated photosynthesis of a canopy is highly
sensitive to V_{cmax} , this simple approach causes considerable distortion in modelled spatial distributions of the terrestrial
carbon cycle (Bonan et al., 2011; Walker et al., 2017; Luo et al., 2017; Chen et al., 2019), hindering advancement in global
45 ecological and Earth system research.

In recent studies, two independent satellite remote sensing approaches have been developed to estimate V_{cmax} at the global
scale. Since the first demonstration of sun-induced chlorophyll fluorescence (SIF) as a proxy of gross primary productivity
(GPP) at the global scale (Frankenberg et al., 2011), the use of SIF for global carbon cycle estimation has been a highly
50 active research field (Mohammed et al., 2019). He et al. (2019) attempted the first global mapping of V_{cmax} from SIF after
converting SIF observations into GPP that is related to V_{cmax} . A time series of daily V_{cmax} maps was derived using SIF
measured by the Global Ozone Monitoring Experiment-2 (GOME-2) sensor from 2007 to 2017 at 36 km resolution (see
Methods). The second space-based approach to deriving V_{cmax} is via leaf chlorophyll content (LCC). Chlorophyll harvests
light that provides energy for the reactions in the Calvin–Benson–Bassham (CBB) cycle of photosynthesis, and therefore is
55 likely coordinated with leaf carboxylation capacity (V_{cmax}) as plants optimize their photosynthetic nitrogen resources (Croft
et al., 2017). The retrieval of LCC from satellite imagery offers the means of reliable and accurate LCC estimation over
different spatiotemporal scales. Data from the MEdium Resolution Imaging Spectrometer (MERIS) in red, near infrared, and
red-edge bands at 300 m resolution at 7-day intervals have been used to produce a global LCC map series from 2003 to 2012
(Croft et al., 2020). In a temperate broadleaf forest, it was found that LCC is better correlated with V_{cmax} than leaf nitrogen
60 content (LNC) over a growing season (Croft et al., 2017), and similar correlations between V_{cmax} and LCC were established
from empirical data for various PFTs (Luo et al., 2020; Lu et al., 2020). In this study, we use this new LCC time series with
existing empirical LCC- V_{cmax} relationships to derive another independent source of information for global V_{cmax} assessment.

The V_{cmax} products derived from SIF and LCC have different strengths and weaknesses. SIF contains strong signals for V_{cmax}
65 because it is directly related to the vegetation photosynthesis rate, but the spatial and temporal resolutions of existing satellite

SIF observations are low. LCC can be derived reliably from multispectral satellite data at much higher spatial and temporal resolutions than those of SIF. Chlorophyll pigments have broad absorption features in the visible range and also affect the fine positioning of red-edge wavelengths. However, the derivation of LCC from remote sensing data is influenced by errors in vegetation structural parameters used in the derivation. The conversion from LCC to V_{cmax} depends on empirical relationships for different PFTs, which have considerable uncertainties (Luo et al., 2019). In order to make the best use of available satellite data for mapping V_{cmax} , we combined SIF and LCC data to produce a single global V_{cmax} time series. We derived a global V_{cmax} time series using SIF data from the TROPical Ozone Mission (TROPOMI) at 0.1° resolution in daily intervals for 2018 with LCC-derived V_{cmax} as a constraint in the derivation using a parameter optimization technique (He et al., 2019; see also Methods). The constraint is made with LCC-derived V_{cmax} aggregated to each 0.1° grid every 7 days as the initial value, which is then replaced when good quality TROPOMI SIF data are available. In this way the best information on V_{cmax} from both SIF and LCC is combined. The combined global V_{cmax} product is highly correlated with that produced from LCC ($r^2=0.90$, $\text{RMSE}=10.82 \mu\text{mol m}^{-2}\text{s}^{-1}$, $P<0.001$), suggesting that much of the LCC information is transferred to this product by filling in its data gaps.

The global distribution of V_{cmax} has also been derived theoretically. Based on a new ecological optimality theory (Wang et al., 2017), Smith et al. (2019) calculated a global V_{cmax} map from meteorological variables of radiation, air temperature and vapor pressure deficit using a monthly climate dataset (Harris et al., 2014). The theory proposes that leaves optimize the use of available resources so that the photosynthetic rate limited by V_{cmax} equals that limited by the electron transport to generate ribulose-1,5,-bisphosphate (RuBP) needed in photosynthesis under average daytime conditions. In this theory, the electron transport rate is computed from meteorological conditions, and is independent of soil nutrient and water conditions. Evaluation against 3672 ground observations shows that the model can capture about 2/3 of the variance in the observed V_{cmax} ($r^2=0.65$, $\text{RMSE}=13.38 \mu\text{mol m}^{-2}\text{s}^{-1}$, $P<0.001$), while the model bias is most significantly correlated to leaf nitrogen content among several leaf and soil parameters (Smith et al., 2019). The validity and reliability of V_{cmax} information derived from the theory are yet to be evaluated outside of the limited amount of ground data.

Here we provide assessment of the reliability of these products for global ecological and Earth system studies. The specific objectives of this study are: (1) to derive new global V_{cmax} products using satellite data; (2) to assess the accuracy of these products against a ground-based dataset; (3) to mutually assess these products; and (4) to evaluate the V_{cmax} product derived ecological optimality theory using satellite-derived V_{cmax} products, as the theory would be useful for estimating V_{cmax} in prognostic terrestrial ecosystem models (TEMs) which are often used in Earth system models.

2. Methods

2.1. Deriving V_{cmax} from SIF

During photosynthesis, plant leaves dissipate part of the excess light energy that is not used in photochemistry in the form of chlorophyll fluorescence (Porcar-Castell et al., 2014). Under conditions without strong moisture and/or thermal stress, the SIF emission from a leaf ~~increases with~~ is approximately proportional to its instantaneous photosynthetic rate (Frankenberg et al., 2011; Guanter et al., 2014; Sun et al., 2014; Li et al., 2018; Wang et al., 2020), although SIF signals are small (1-5% of reflected radiation at near infrared wavelengths, Colombo et al., 2016) and contain noise from various sources including the variations in solar illumination angle and sensor view angle (Dechant et al., 2020). In a plant canopy, sunlit leaves are the predominant sources of SIF (Pinto et al., 2016). For the purpose of deriving leaf-level information, the total SIF measured from a canopy was first separated into sunlit and shaded leaf components according to sun-target-sensor observation geometry and canopy architectural parameters. The observation geometry was determined by satellite and solar zenith and azimuthal angles. The main canopy architectural parameters were leaf area index (LAI), which quantifies the amount of leaf area in the canopy per unit ground surface area, and the clumping index (CI), which characterizes the non-random spatial distribution of leaves in the canopy. Both LAI and CI were used to separate sunlit and shaded leaf fractions in the canopy, and the observation geometry determined the proportion of sunlit leaves observed by a satellite sensor (Chen et al., 1999). Leaf reflectance at the SIF wavelength was used to estimate the strength of multiple scattering of emitted SIF in the canopy that enhances SIF observed from sunlit leaves (He et al., 2019). The sunlit SIF component derived in this way was then converted into the average sunlit leaf photosynthetic rate, from which V_{cmax} is derived using a data assimilation-~~data assimilation~~ technique (He et al., 2019). An ensemble Kalman filter (EnKF) was developed using an ecosystem model (Chen et al., 2012) and used in the data assimilation technique to optimize V_{cmax} based on the difference between SIF-derived and modeled average sunlit leaf photosynthetic rates. In the optimization, it was assumed that the error in modelling the photosynthetic rate was caused by both inaccuracy in the initial V_{cmax} input (constants by PFT or estimated based on LCC) and the collective errors in other parameters including environmental conditions (meteorology and soil) used in the model. An error matrix was therefore developed to determine the amount of adjustment to the initial V_{cmax} value (He et al., 2019). Optimized V_{cmax} values often differed considerably from the initialized values beyond their error ranges, suggesting that SIF observations provided reliable and strong signals for its optimization, even though other model errors are also present.

The data assimilation methodology was first applied to GOME-2 SIF data and generated a global daily V_{cmax} map series from 2007 to 2017 at 36 km resolution (He et al., 2019). In this study, this methodology was refined and applied to TROPOMI SIF data to produce global daily V_{cmax} maps in 2018 at 0.1° resolution (approximately 10 km). The refinements included the conversion from SIF to GPP using non-linear relationships (Liu et al., 2022) rather than linear relationships used in He et al. (2019) and the initialization of V_{cmax} using the LCC product (Croft et al., 2020) rather than constant V_{cmax} by PFT. Although the ~~TROPOMI~~- V_{cmax} map series produced using TROPOMI SIF + LCC data is available for only one year, it has a much higher spatial resolution than that produced from GOME-2, and therefore has broader applications in global ecological research.

2.2. Deriving V_{cmax} from LCC

LCC is responsible for light harvesting and providing excitation energy to drive photosynthesis in leaves, while V_{cmax} defines the capacity of leaves to utilize the excitation energy for photosynthesis. These two leaf traits are dynamically optimized to local environmental conditions to achieve an optimal use of nitrogen resources (Xu et al., 2012). LCC is a relatively stable trait without much day-to-day and diurnal variations, while V_{cmax} is sensitive to temperature. Empirical data show close relationships between LCC and $V_{\text{cmax}25}$ (Houburg et al., 2013; Croft et al., 2017; Lu et al., 2020), which is V_{cmax} normalized to its value at 25°C using a temperature function (Smith et al., 2019, see also Section 2.4 below). A two-step radiative transfer model inversion method was developed for retrieving LCC from multispectral satellite data (Zhang et al., 2008; Croft et al., 2020). In step 1, the canopy-level reflectance was inverted to leaf-level reflectance with a look-up-table (LUT) constructed using canopy radiative transfer model for canopies with turbid media (Verhoef, 1984) and a geometrical optical model for clumped canopies (Chen and Leblanc, 1997 and 2001) that computed observed sunlit leaf fraction according to canopy structure and sun-target-view geometry. In step 2, the leaf-level PROSPECT model (Feret et al., 2008) was inverted to obtain LCC from the inverted multi-spectral leaf reflectance. This two-step model inversion algorithm avoids issues with empirical methods that directly link LCC to canopy-level remote sensing data, which lack generality because of variable canopy structure and sun-target-view geometry. The first time-series of global LCC maps were retrieved using MERIS data from 2003 to 2011 at 300 m resolution and 7-day intervals (Croft et al., 2020). A validation using 248 ground sites in 5 PFTs suggests that this product is reliable ($r^2=0.5$, $p<0.01$, $\text{RMSE}=10.79 \mu\text{g cm}^{-2}$ or mean error 23%). Using empirical relationships between LCC and $V_{\text{cmax}25}$ for various PFTs (Luo et al., 2019), this global LCC time series was converted into $V_{\text{cmax}25}$.

2.3. Ground-based V_{cmax} dataset

In this study, we use the same ground-based V_{cmax} dataset as that used by Smith et al. (2019). It consisted of 3672 entries for 1474 plant species that are grouped into 7 PFTs in this study. Each entry consisted of V_{cmax} measured from one or more leaves with companion data of air temperature, humidity, incoming PAR, longitude and latitude. V_{cmax} was derived from several pairs of photosynthesis (A) and intercellular CO_2 concentration (C_i) (to construct an A/C_i curve) (56%) or from a single pair of A and C_i using the method of De Kauwe et al. (2016) (44%).

To match with V_{cmax} maps derived from SIF, LCC and EOT, the ground-based data were aggregated in two ways: (1) the data points of the same PFT as that in the PTF map (Figure 4b) used for LCC and SIF processing were grouped to form an average V_{cmax} for a grid, while mismatched datapoints within the grid were ignored, and (2) all existing data points within each grid were averaged and labelled as the dominant PFT. We found that second way resulted in better correlation with all three types of V_{cmax} maps. After the aggregation to 0.5° resolution, there were 180 data points for all PFTs used in the final analysis of all V_{cmax} products.

2.4. Temperature normalization

For the same leaf, V_{cmax} varies exponentially with leaf temperature, and hence it is more meaningful to compare $V_{\text{cmax}25}$ between leaves or different estimates. In this study, all global V_{cmax} products are derived at the growth temperature. To facilitate their comparisons with ground databases and their future use in models, V_{cmax} is converted to $V_{\text{cmax}25}$ using a
170 common temperature function (Eq. 22 in Smith et al., 2019).

3. Results

3.1. Evaluation of Four Global V_{cmax} Products

The global distributions of the growing season mean V_{cmax} obtained from GOME-2 SIF, MERIS LCC and TROPOMI SIF are shown in Figure 1 in comparison with V_{cmax} calculated from the ecological optimality theory (EOT) at the growing
175 season mean temperature. For this comparison, $V_{\text{cmax}25}$ derived from LCC is converted to V_{cmax} at the mean growing temperature. The growing season is defined as the period when monthly mean air temperature is above 0°C. These four global V_{cmax} distributions derived at different spatial resolutions at 36 km, 300 m, 0.1° and 0.5° from GOME-2 SIF, LCC, TROPOMI SIF and EOT, respectively, and aggregated to 0.5° resolution in Figure 1, are highly correlated spatially, although their details differ to some extent. The distribution derived from the optimality theory appears to be spatially smooth,
180 reflecting the fact that meteorological variables used for V_{cmax} prediction do not vary abruptly in space. The three remote sensing products show mutually-consistent patchy patterns, suggesting that they have all captured some realistic variability on the ground associated with PFT distribution patterns. However, all four products show remarkable similarities in the overall geographic patterns and mutually well correlated with each other ($R^2=0.76-0.90$, $p<0.001$). Among three remote sensing products, SIF-derived products correlate best with the product based on the ecological optimality theory (EOT)
185 ($r^2=0.85$, $\text{RMSE}=11.69 \mu\text{mol m}^{-2}\text{s}^{-1}$, $P<0.001$ for GOME-2; $r^2=0.76$, $\text{RMSE}=15.77 \mu\text{mol m}^{-2}\text{s}^{-1}$, $P<0.001$ for TROPOMI). We further evaluate these products below.

All four V_{cmax} products compare well with ground-based measurements (Figure 2) after they are aggregated to the corresponding 0.5° grids (see Methods). The correlation of optimality-based V_{cmax} with the ground measurements is similar
190 to that shown in Smith et al. (2019) ($r^2=0.66$, $\text{RMSE}=13.37 \mu\text{mol m}^{-2}\text{s}^{-1}$, $P<0.001$), and correlations of other three V_{cmax} products with the same ground measurements are similar ($r^2=0.69$, $\text{RMSE}=13.80 \mu\text{mol m}^{-2}\text{s}^{-1}$, $P<0.001$ for GOME-2; $r^2=0.80$, $\text{RMSE}=8.99 \mu\text{mol m}^{-2}\text{s}^{-1}$, $P<0.001$ for TROPOMI; $r^2=0.55$, $\text{RMSE}=18.28 \mu\text{mol m}^{-2}\text{s}^{-1}$, $P<0.001$ for LCC). It is encouraging to see that three of the four products captured about 2/3 of the variance in the ground data, despite the large-scale mismatch between the grids of these products and the ground data points. Some errors would also be expected from
195 temporal mismatches as the differences in the years of ground and remote sensing data acquisitions are not considered (in order to have as many data points as possible in the comparisons), although data outside of the growing season are excluded. While V_{cmax} for individual leaves may vary greatly among plant species within the same functional type and with

environmental conditions over the landscape, their locally averaged values would be expected to display a consistent spatial pattern at large scales that are determined more or less by meteorological conditions – permitting the success of the optimality theory for predicting V_{cmax} based on meteorological variables alone. Coarse-resolution remote sensing data, such as GOME-2 SIF data at 36 km resolution and TROPOMI at 0.1° resolution, can also capture the spatial variability in V_{cmax} at large scales.

The correlation statistics of the four products shown in Figure 2 with the ground database by plant function type are given in Table 1. Forest PFTs of ENF, DNF and DBF are combined in order to have a sufficient number of data points for the statistical analysis. Correlations for most PFTs are highly significant for all products ($p < 0.001$), but for forest PFTs and SHR the correlations are weak for most products except for TROPOMI. The TROPOMI V_{cmax} product (<https://doi.org/10.5281/zenodo.6466968>) compares best with the ground database in terms of the Pearson correlation coefficient (r^2), RMSE and the p value from two-tailed paired T tests, suggesting that the combination of SIF and LCC information is effective in capturing the spatial variability of V_{cmax} for the various PFTs. It is therefore most ready for global ecological studies among the four products.

The V_{cmax} values derived independently from GOME-2 SIF and MERIS LCC at the mean growing season temperature are well correlated overall ($r^2 = 0.79$) and for individual PFTs ($r^2 = 0.77-0.88$) except for EBF ($r^2 = 0.26$) (Figure 3). These high correlations suggest that the signals contained in both SIF and multi-spectral reflectance data used for LCC retrieval are strong and useful for deriving V_{cmax} . This is particularly encouraging because both types of remote sensing data are increasingly available with existing and forthcoming satellite sensors providing improved SIF (Muhammed et al., 2019) and multi-spectral data (such as the Sentinel sensor series, <https://sentinel.esa.int/web/>). The differences between these two independent retrievals of V_{cmax} are still considerable, especially for EBF in the tropics due to frequent cloud cover, and there is room for improvement not only in the retrieval algorithms but also in providing improved SIF and spectral data at higher spatial and temporal resolutions. Much more ground-based data of V_{cmax} , LCC and associated structural parameters (leaf area index and clumping index) are still needed for refining and validating the retrieved V_{cmax} . However, these existing products are already a large step forward from the current state of the art and can be employed immediately for parameterizing and benchmarking TEMs. In other words, these products may have already overcome the V_{cmax} bottleneck in accurate modeling of the spatio-temporal patterns of the terrestrial productivity and carbon cycle.

3.2. Influence of Environmental Factors on V_{cmax}

V_{cmax} values derived from all three remote sensing products shown in Figure 1 are most obviously larger than those produced by EOT over croplands and grasslands in Americas, India and China. [Cropland and grassland management, especially including fertilization and irrigation](#), may explain part of this divergence. To explore the possible influences of

cropland and grassland irrigation on V_{cmax} , we used a global irrigation map (<http://www.fao.org/nr/water/aquastat/irrigationmap/index.stm>) at 0.5° resolution to compare with the relative difference (ΔV_{cmax}) between TROPOMI SIF+LCC V_{cmax} and EOT-based V_{cmax} , i.e. (TROPOMI-EOT)/EOT (Figure 4). Globally, ΔV_{cmax} increases with irrigated area percentage. The regression coefficient (R) between the actual values of percent irrigated area and ΔV_{cmax} for the areas of irrigation greater than 5% at the global scale is +0.26 ($p < 0.001$) and +0.11 ($p < 0.001$) for croplands and grasslands, respectively. In some regions, including China, India and the Middle East, the correlation coefficient is considerably higher (0.25-0.5, $p < 0.001$). [Irrigation in cropland and grassland would reduce water stress and increase leaf photosynthetic capacity \(Reed and Loik, 2016; Chen et al., 2019; Song et al., 2021\), giving rise to the positive correlation between \$\Delta V_{\text{cmax}}\$ and percent of irrigation area in a pixel. For crops, fertilization would generally co-occur with irrigation \(Sela, 2021\), so this positive correlation could also include the effect of fertilization on \$V_{\text{cmax}}\$.](#)

Soil properties may also influence V_{cmax} (Reich et al., 2007, Maire et al., 2015; Ali et al., 2015, Smith and Dukes, 2018). Among soil properties available in the global SoilGrids database (Hengl et al., 2017), we found that soil pH best correlates with ΔV_{cmax} . Soil pH is spatially variable (Figure 5a), and we found that ΔV_{cmax} is positively and significantly correlated to soil pH in most regions, with 43% (11970 out of 27681 pixels) of cropland and grassland areas having $R > 0.1$ and $p < 0.1$ (Figure 5). Similar statistics are found for other PFTs, suggesting that soil pH has similar effects on V_{cmax} across PFTs. However, ΔV_{cmax} is not significantly correlated with other soil properties, including soil carbon content, nitrogen content and cation exchange capacity. Soil pH is a key control on soil biochemical reactions affecting nutrient uptake (Hall et al., 1998) and has an optimum range for plant growth from 5.5 to 7.5 (Islam 1980). As soil pH varies in a wide range (4 to 8, Figure 5), its effect on V_{cmax} is therefore detectable from remote sensing signals. Plants on acidic soils tend to have higher ratios of leaf-internal to ambient CO_2 (Wang et al., 2017; Dong et al., 2020; Pailassa et al. 2020) and therefore would be expected to have lower V_{cmax} . These results suggest that V_{cmax} derived from SIF has captured much of the spatial variability in V_{cmax} due to irrigation and soil properties that are not captured by optimality theory. Remote sensing products can therefore provide more nuanced information on plant responses to non-meteorological environmental drivers and can therefore provide more accurate V_{cmax} estimates and additional information on its spatial variability.

In addition to soil properties, leaf traits are expected to be more directly related to V_{cmax} . We use LCC, which contains part of the leaf photosynthetic nitrogen pool (Xu et al., 2012), as an indicator of the effect of leaf traits on V_{cmax} . We found that ΔV_{cmax} is significantly and positively correlated to LCC for individual PFTs ($r^2 = 0.01-0.27$, $P < 0.001$ for TROPOMI) and for all PFTs combined ($r^2 = 0.10$, $P < 0.001$) (Figure 6). Similarly, the relative difference in EOT-derived V_{cmax} and ground measurements is also significantly correlated with leaf nitrogen content ($r^2 = 0.21$, $P < 0.001$, Figure 7), in agreement with the finding of Smith et al. (2019). These positive relationships suggest that LCC as a proxy of the photosynthetic nitrogen content in leaves can explain part of the spatial variability in V_{cmax} due to the variations in environmental conditions that are

not captured by the optimality theory. The added information from LCC due to plants' optimal allocation of nutrient resources would be useful to improve optimality-based modeling of V_{cmax} .

The global distribution patterns of growing season V_{cmax} shown by the four products (Figure 1) have common latitudinal gradients, i.e. V_{cmax} is generally largest near the equator and decreases away from the equator. This latitudinal dependence is simulated in EOT through considering radiation, i.e. stronger radiation leading to larger V_{cmax} . This influence of radiation on V_{cmax} is well captured by the three remote sensing products. According to analyses of the leaf economics spectrum (Wright et al., 2004; Sack et al., 2013; Osnas et al., 2013; Reich 2014), leaf photosynthetic capacity increases with mean annual rainfall, and therefore V_{cmax} in dry areas is expected to be smaller than that in wet areas. However, several semi-arid regions, such as India, middle East, southeast Brazil, and areas near the southern border of the Sahara desert, have large V_{cmax} values. We found that these are mostly irrigated agricultural areas (Figure 4) and the high V_{cmax} values there are due to crop management and are not in contradiction to existing leaf economics spectrum data. The V_{cmax} distribution pattern in Australia is compatible with the rainfall distribution, i.e. the lowest V_{cmax} is found in central Australia where rainfall is lowest and the highest V_{cmax} is located in northern Australia where rainfall is largest. The EOT product can also capture this pattern to some extent through meteorological variables (e.g. radiation and temperature). There are many spatial details in these V_{cmax} products that are of great interest to leaf economic studies.

3.3. Global Mean Values of V_{cmax} for Different Biomes

We compared the mean V_{cmax} values of the TROPOMI SIF+LCC product, denoted by $V_{\text{cmax}T_g}$, representing the three remote sensing products, and the EOT product over the growing season grouped by PFT with ground-based datasets at the mean growth temperature and at 25 °C after temperature normalization using the same scheme of Smith et al. (2019) (Table 2). The agreement between TROPOMI and EOT is best for EBF, DBF, SHR and GRS, for which the difference between the two products is smaller than their mean standard deviation. For ENF, DNF and CRP, the difference between the two products exceeded their mean standard deviation. TROPOMI $V_{\text{cmax}T_g}$ is also considerably smaller than the ground datasets because of the large contributions of high latitude conifer forests with low $V_{\text{cmax}T_g}$ that are underrepresented in the ground datasets (Figure 8). Since the TROPOMI $V_{\text{cmax}T_g}$ product compares well with the ground database (Figure 1 and Table 1) and has complete coverage for each PFT, it provides more reliable global averages than the ground database shown in Table 2. Ground data for DNF are too few (Figure 8) to make sound evaluation for this PTF. TROPOMI $V_{\text{cmax}T_g}$ is considerably larger than EOT $V_{\text{cmax}T_g}$ for CRP, as well as GRS to a less extent, mostly because of the positive impact of irrigation on $V_{\text{cmax}T_g}$ as demonstrated in Figure 4. Although the same temperature function is used in the normalization for all products, the relative changes from $V_{\text{cmax}T_g}$ to $V_{\text{cmax}25}$ for the various PFTs differed slightly among the four global products (Table 2) as the differences in $V_{\text{cmax}T_g}$ among the products vary spatially with different growth temperatures, creating different weights in the calculation of the global averages of $V_{\text{cmax}25}$.

In addition to the TROPOMI V_{cmax} product, the other two remote sensing products are also compared in Figure 9. The magnitude of $V_{\text{cmax}25}$ in the TROPOMI product is generally in between those from GOME-2 SIF and LCC for the various PFTs (Figure 9a) because it uses information of LCC which tends to be converted to lower values of V_{cmax} using existing empirical relationships. For forest PFTs, both $V_{\text{cmax}25}$ and $V_{\text{cmax}Tg}$ of the EOT product is generally larger than those of remote sensing products. This is likely due to the fact that EOT considers only meteorological variables while soil nutrients and other variables could impose limitations on plant growth and hence leaf traits while remote sensing techniques could be responsive to these soil effects on plants. For the same reason, $V_{\text{cmax}25}$ and $V_{\text{cmax}Tg}$ values of the EOT product for CRP is smaller than those of remote sensing products because crop irrigation and soil pH could have positive effects on leaf V_{cmax} that are captured by the remote sensing products but not by EOT (Figures 3 and 4). The mean values of $V_{\text{cmax}25}$ and $V_{\text{cmax}Tg}$ from the ground databases (Smith et al., 1999; Kattge et al., 2009) are given in Figure 9 for comparison purposes, but they don't represent the true global averages for the various PFTs because of their limited spatial distributions (Figure 8 for Smith et al., 2019). We therefore don't yet have true ground averages to determine which product provides the most reliable global averages for the various PFTs. However, based on the point-to-point comparisons (Figure 1 and Table 1), we believe that the TROPOMI product is most reliable in providing the global averages of $V_{\text{cmax}25}$ and $V_{\text{cmax}Tg}$ for the various PFTs.

4. Discussion

The V_{cmax} datasets derived from SIF and LCC represent the *in situ* leaf-level V_{cmax} that is the collective outcome of meteorological conditions and other environmental properties. These datasets can therefore be used directly in TEMs without further adjustment. The TRY database (Kattge et al., 2009) contains both V_{cmax} normalized to 25°C ($V_{\text{cmax}25}$) and total LNC, and they are well correlated. Empirical studies have also shown this correlation (Ryan, 1995; Medlyn et al., 1999; Walker et al., 2014; Prentice et al., 2014). LNC has therefore been used to adjust $V_{\text{cmax}25}$ within the same PFT in some TEMs. However, such an adjustment can only recover part of the spatio-temporal variability in $V_{\text{cmax}25}$ because only a small part of LNC is closely linked to carboxylation capacity. LNC can be separated into four components: photosynthetic, structural, storage and respiratory nitrogen pools (Xu et al., 2012; Ali et al., 2016). The photosynthetic nitrogen pool can be further divided into sub-pools for light harvesting, electronic transport and carboxylation, and its fraction to the total LNC is variable depending on meteorological and soil conditions and possibly also atmospheric CO₂ concentration (Ali et al., 2016). For fully grown leaves in balance with environmental conditions, these sub-pools are naturally optimized so that the investment of resources in light-harvesting optimally satisfies the need for electron transport or carboxylation (Xu et al., 2012). In other words, photosynthetic subpools are highly correlated, giving rise to the experimental evidence that LCC containing the light-harvesting nitrogen is highly correlated to V_{cmax} and J_{max} (Croft et al., 2017). The daunting and complex task of mapping the spatio-temporal distributions of leaf photosynthetic capacity could therefore be accomplished by mapping LCC that contains nitrogen in balance with carboxylation nitrogen in Rubisco, and multispectral or hyperspectral remote sensing data that are highly sensitive to light absorption by the chlorophyll pigments would be a reliable way to obtain such highly desirable

330 information. The LCC product shown in this study could therefore be used in conjunction with V_{cmax} products derived from SIF and optimality theory to parameterize V_{cmax} models with consideration of the nitrogen cycle.

335 Our remote sensing algorithms derive V_{cmax} from SIF and LCC from multi-spectral data from sunlit leaves after considering the Sun-target-view geometry (He et al., 2019; Croft et al., 2020), and hence the remote sensing V_{cmax} products represent sunlit leaves observed by the sensors. The observed sunlit leaves are mostly located near the top of the canopy, and hence these V_{cmax} products could be considered to represent the average condition of leaves near the top of the canopy. In applying a V_{cmax} value to a canopy, it would be necessary to consider the vertical variation of V_{cmax} in the canopy. A mathematical scheme to integrate the vertical variation for average sunlit and shaded leaves at different LAI values and solar zenith angles is available from Chen et al. (2012).

340 The growing season mean V_{cmax} products are available at <https://doi.org/10.5281/zenodo.6466968>, but seasonal variation of V_{cmax} is not yet ready for distribution. Reliable seasonal variation of V_{cmax} is not yet produced at the global scale due to several reasons: (1) SIF data are often not reliable over non-growing seasons and near the beginning and end of the growing season; (2) LCC derivation is considerably affected by the inaccuracy in the input LAI data outside of the growing season, and near the beginning and end of the growing season the separation of LCC and LAI signals in remote sensing data is still an issue; (3) the ecological optimality theory that provides the basis for evaluating remote sensing V_{cmax} products can so far be used for calculating growing season mean V_{cmax} and is not yet ready for calculating its seasonal variation; and (4) few ground-based data with seasonal variation of V_{cmax} are available for validation. While efforts are being made to overcome these issues, it will take a while to accumulate sufficient ground-based datasets and to improve remote sensing algorithms and the optimality theory before reliable seasonal variation of V_{cmax} can be derived at the global scale.

345
350

5. Conclusion

The two RS V_{cmax} products used in this research were derived independently from separate satellite observations of SIF and LCC, and yet show close agreement in their magnitudes and spatial patterns of modelled V_{cmax} . These remotely sensed V_{cmax} products (<https://doi.org/10.5281/zenodo.6466968>) also closely agree in large-scale spatial patterns with those calculated from the ecological optimality theory using meteorological variables, providing support for the use the theory for prognostic modeling of terrestrial ecosystem function under future climate scenarios. However, the optimality-based V_{cmax} product does not show the local-scale spatial distribution patterns that are consistently found in all three remote sensing products because of patchy land cover distributions, implying that meteorological variables alone do not capture all spatial variability. Importantly, the relative difference in V_{cmax} (ΔV_{cmax}) between SIF and optimality-based products is found to be significantly correlated to the fraction of irrigation area in a pixel, soil pH and leaf nitrogen content; highlighting the impacts of environmental conditions on V_{cmax} that are not captured within optimality theory. From these results, we conclude: (1) the

355
360

remote sensing products shown in this study have reliably captured the spatial variability in V_{cmax} and therefore are directly useful for diagnostic ecological modeling at the global scale, and (2) in comparison to the optimality-based product, the remote sensing products provide additional information on how V_{cmax} varies according to local environmental conditions, which is useful for prognostic modeling purposes. Furthermore, understanding the dynamic in situ response of plant photosynthetic capacity to soil water and nutrient availability, independent of meteorological drivers, is important to monitoring plant photosynthetic potential. The LCC product shown in this study could be used in conjunction with V_{cmax} products derived from SIF and optimality theory to parameterize V_{cmax} models with consideration of the nitrogen cycle. This work demonstrates the power of global-scale satellite-based and ecological optimality approaches to reveal crucial spatial information on V_{cmax} ; thereby removing a barrier in global ecological and Earth system research.

References

- Ali, A.A., Xu, C., Rogers, A., Fisher, R.A., Wullschleger, S.D., Massoud, E.C., ... Wilson, C. J.: A global scale mechanistic model of photosynthetic capacity (LUNA V1.0). *Geoscientific Model Development*, 9(2), 587–606, 2016.
- Ali, A.A., Xu, C., Rogers, A. et al.: Global-scale environmental control of plant photosynthetic capacity. *Ecological Applications*, **25**, 2349–2365, 2015.
- Bonan, G.B., Lawrence, P.J., Oleson K.W. et al.: Improving canopy processes in the Community Land Model version 4 (CLM4) using global flux fields empirically inferred from FLUXNET data. *Journal of Geophysical Research: Biogeosciences*, **116**, G02014, 2011.
- [Chen, B., Chen, J. M., Baldocchi, D. D., Liu, Y., Zheng, T., Black, T. A. and Croft, H.: A new way to include soil water stress in terrestrial ecosystem models. *Agricultural and Forest Meteorology*, 276, 107649, <https://doi.org/10.1016/j.agrformet.2019.107649>, 2019.](https://doi.org/10.1016/j.agrformet.2019.107649)
- Chen, J.M., Liu, J., Cihlar, J. and Guolden, M.L.: Daily canopy photosynthesis model through temporal and spatial scaling for remote sensing applications. *Ecological Modelling*, 124: 99-119, 2019.
- Chen, J.M., and Leblanc, S.G. (1997). A 4-scale bidirectional reflection model based on canopy architecture. *IEEE Transactions on Geoscience and Remote Sensing*, 35: 1316-1337.
- Chen, J.M., and Leblanc, S.G.: Multiple-scattering scheme useful for hyperspectral geometrical optical modelling. *IEEE Transactions on Geoscience and Remote Sensing*, 39(5): 1061-1071, 2001.
- Chen, J.M., Mo, G., Pisek, J., Deng, F., Ishozawa, M. and Chan, D.: Effects of foliage clumping on global terrestrial gross primary productivity. *Global Biogeochemical Cycles*, VOL. 26, GB1019, 18 PP., doi:10.1029/2010GB003996, 2012.
- Chen, J. M., Ju, W., Ciais, P., Viovy, N., Liu, R. and Liu, Y.: Vegetation structural change since 1981 significantly enhanced the terrestrial carbon sink. *Nature Communications*, 10:4259 | <https://doi.org/10.1038/s41467-019-12257-8>, 2019.

- Chen, J. M., Wang, R., Liu, Y., He, L., Croft, H., Luo, X., Wang, H., Smith, N. G., Keenan, T. F., Prentice, I. C., Zhang, Y.,
395 Ju, W. and Dong N.: Three global products of leaf photosynthetic capacity derived from satellite observations.
<https://doi.org/10.5281/zenodo.6466968>. 2022.
- [Colombo, R., M. Meroni, M. Rossini, 2016. Development of fluorescence indices to minimize the effects of canopy
structural parameters. *Annali Di Botanica*, 6:93-99.](#)
- Croft, H., Chen, J.M., Luo, X.Z., Bartlett, P., Chen, B. & Staebler, R.M.: Leaf Chlorophyll Content as a Proxy for Leaf
400 Photosynthetic Capacity. *Global Change Biology*, 23 (9):3513-3524. doi:10.1111/gcb.13599, 2017.
- Croft, H., Chen, J.M., et al.: Global distribution of leaf chlorophyll content. *Remote Sensing of Environment*, 236, 111479,
2020.
- [Dechant, B., Y. Ryu, G. Badgley, Y. Zeng, J. A. Berry, Y. Zhang, T. Goulas, Z. Li, Q. Zhang, M. Kang, J. Li, and I. Moya.
2020. Canopy structure explains the relationship between photosynthesis and sun-induced chlorophyll fluorescence in
405 crops. *Remote Sensing of Environment*, 241, 111733.](#)
- De Kauwe, M.G., Lin, Y., Wright, I.J., Medlyn, B.E., Crous, K.Y., Ellsworth, D.S. et al.: A test of the ‘one-point method’
for estimating maximum carboxylation capacity from field-measured, light saturated photosynthesis. *New Phytologist*,
210, 1130–1144, 2016.
- Dong, N., Prentice, I. C., Wright, I. J., Evans, B. J., Togashi, H. F., Caddy-Retalic, S., . . . Lowe, A. J.: Components of leaf-
410 trait variation along environmental gradients. *New Phytologist*, 228(1), 82-94. doi:<https://doi.org/10.1111/nph.16558>,
2020.
- Farquhar, G.D., von Caemmerer, S. and Berry, J.A.: A biochemical model of photosynthetic CO₂ assimilation in leaves of
C₃ species. *Planta*, 149, 78-90, 1980.
- Feret, J.B., François, C., Asner, G.P., Gitelson, A.A. et al.: PROSPECT-4 and 5: Advances in the leaf optical properties
415 model separating photosynthetic pigments. *Remote Sensing of Environment*, 112, 3030-3043, 2008.
- Fisher, J.B., Badgley, G. and Blyth, E.: Global nutrient limitation in terrestrial vegetation. *Global Biogeochemical Cycles*.
26, GB3007, 2012.
- Frankenberg, C., Fisher, J.B., Worden, J., Badgley, G., Saatchi, S.S., Lee, J.E., and Kuze, A.: New global observations of
the terrestrial carbon cycle from GOSAT: Patterns of plant fluorescence with gross primary productivity. *Geophysical
420 Research Letters*, 38, L17706, 2011.
- Gentili, R., Ambroshin, R., Montagnani, C., Caronni S., & Citterio, S.: Tffect of soil pH on the growth, reproductive
investment and pollen allergenicity of *Ambrosia artemisiifolia* L. *Frontiers of Plant Science*, 9, 1335, 2018.
- Guanter, L., Zhang, Y., Jung, M., Joiner, J., Voigt, M., Berry, J.A., et al.: Global and time-resolved monitoring of crop
photosynthesis with chlorophyll fluorescence. *Proceedings of the National Academy of Sciences*, 111(14), E1327-E1333,
425 2014.
- Hall, J.M., Paterson E. and Killham, K.: The effect of elevated CO₂ concentration and soil pH on the relationship between
plant growth and rhizosphere denitrification potential. *Global Change Biology*, 4: 209-216, 1998.

- Harris, I., Jones, P.D., Osborn, T.J. and Lister, D.H.: Updated high resolution grids of monthly climatic observations – the CRU TS3.10 Dataset. *Int. J. Climatol.*, 34, 623–642, 2014.
- 430 He, L., Chen, J.M., Liu, J., Zheng, T., Wang, R., Joiner, J., Chou, S., Chen, B., Liu, Y., and Liu, R.: Diverse photosynthetic capacity of global ecosystems mapped by satellite chlorophyll fluorescence measurements. *Remote Sensing of Environment*, 232, 111344, 2019.
- Hengl, T., de Jesus, J.M., Heuvelink, G.B., et al.: SoilGrids250m: Global gridded soil information based on machine learning. *PLoS ONE*, 12(2): e0169748, 2017
- 435 Houborg, R., Cescatti, A., Migliavacca, M., & Kustas, W.P.: Satellite retrievals of leaf chlorophyll and photosynthetic capacity for improved modeling of GPP. *Agricultural and Forest Meteorology*, 177, 10 – 23, 2017.
- Islam, A.K.M.S., Edwards D.G., and Asher, C.J.: pH optima for crop growth: results of a flowing solution culture experiment with six species. *Plant and Soil*, 54: 339-357, 1980
- Kattge, J., Knorr, W., Raddatz, T. and Wirth, C.: Quantifying Photosynthetic Capacity and Its Relationship to Leaf Nitrogen
440 Content for Global-Scale Terrestrial Biosphere Models. *Global Change Biology*, 15 (4):976-991., 2009.
- Kattge, J., Bönišch, G., Díaz, S., Lavorel, S., Prentice, I.C., Leadley, P., et al. (2020). TRY plant trait database – enhanced coverage and open access. *Global Change Biology* **26**, 119–188.
- Li, X., Xiao, J., He, B., Arain, M.A., Beringer, J., Desai, A.R., et al.: Solar-induced chlorophyll fluorescence is strongly correlated with terrestrial photosynthesis for a wide variety of biomes: first global analysis based on OCO-2 and flux
445 tower observations. *Global Change Biology*, 24:3990–4008, 2018.
- Liu, Y., Chen, J.M., He, L., Zhang, Z., Wang, R., Rogers, C., Fan, F., de Oliveira, G., and Xie, X.: Non-linearity between gross primary production and far-red solar-induced chlorophyll fluorescence emitted from major biomes. *Remote Sensing of Environment* 271, 112896, 2022.
- Lu, X., Ju, W., Li, J., Croft, H., Chen, J.M., and Luo, Y.: Maximum carboxylation rate estimation with chlorophyll content
450 as a proxy of RuBisCo. *Journal of Geophysical Research: Biogeosciences*. 125(8), e2020JG005748, 2020.
- Luo, X., Croft, H., Chen, J.M., Bartlett, P., Staebler, R. and Froelich, N.: Incorporating leaf chlorophyll content into a terrestrial biosphere model for estimating carbon and water fluxes at a forest site. *Agricultural and Forest Meteorology*, 248: 156-168, 2017.
- Luo, X., Croft, H., Chen, J.M., He, L. and Keenan, T.F.: Improved estimation of global photosynthesis using information on
455 leaf chlorophyll content. *Global Change Biology*, 25(7), GCB14624, 2019.
- Maire V., Prentice, I.C. et al.: Global effects of soil and climate on leaf photosynthetic traits and rates. *Global Ecology and Biogeography*, 24(6), GEB12296, 2015.
- Medlyn, B.E., Badeck, F.-W., De Pury, D.G.G., et al.: Effects of elevated [CO₂] on photosynthesis in European forest species: a meta analysis of model parameters, *Plant Cell Environ.*, 22, 1475–1495, 1999.
- 460 Mohammed, G.H., Colombo, R., Middleton, E. et al.: Remote sensing of solar-induced chlorophyll fluorescence (SIF) in vegetation: 50 years of progress. *Remote Sensing of Environment*, 231: 111177, 2019.

- Osnas, J. L. D., Lichstein, J. W., Reich, P. B., and Pacala, S. W.: Global leaf trait relationships: mass, area, and the leaf economics spectrum. *Science*, 340, 741-744, 2013.
- Paillassa J., Wright, I.J., Prentice, I.C., Pepin, S., and Smith, N.G.: When and where soil is important to modify the carbon and water economy of leaves. *New Phytologist*, 15, NPH16702, 2020.
- 465 [Pinto, F., Damm, A., Schickling, A., Panigada, C., Cogliati, S., Muller-Linow, M., ... Rascher, U., 2016. Sun-induced chlorophyll fluorescence from high-resolution imaging spectroscopy data to quantify spatio-temporal patterns of photosynthetic function in crop canopies. *Plant Cell and Environment*, 39 \(7\), 1500–1512.](#)
- Porcar-Castell, A., Tyystjärvi, E., Atherton, J., van der Tol, C., Flexas, J., Pfündel, E.E., et al.: Linking chlorophyll a
470 fluorescence to photosynthesis for remote sensing applications: Mechanisms and challenges. *Journal of Experimental Botany*, 65(15), 4065-4095, 2014.
- Prentice, I.C., Dong, N., Gleason, S.M., Maire, V., and Wright, I.J.: Balancing the costs of carbon gain and water transport: testing a new theoretical framework for plant functional ecology, *Ecol. Lett.*, 17, 82–91, 2014.
- 475 [Reed, C. C. and Loik, M. E.: Water relations and photosynthesis along an elevation gradient for *Artemisia tridentata* during and historic drought. *Oecologia*, doi: 10.1007/s00442-015-3528-7, 2016.](#)
- Reich, P.B., Wright, I.J., and Lusk, C.H.: Predicting leaf physiology from simple plant and climate attributes: a global GLOPNET analysis. *Ecological Applications*, 17, 1982–1988, 2007.
- 480 [Reich, P. B.: The world-wide “fast-slow” plant economics spectrum: a traits manifesto. *Journal of Ecology*, 102: 275-301, 2014.](#)
- Rogers, A.: The use and misuse of Vc, max in Earth System Models. *Photosynthesis Research*, 119, 15–29, 2014.
- Rogers, A., Medlyn, B.E., Dukes, J.S. et al.: A roadmap for improving the representation of photosynthesis in Earth system models. *New Phytologist*, 213, 22–42, 2017.
- Ryan, M.G.: Foliar maintenance respiration of subalpine and boreal trees and shrubs in relation to nitrogen concentration, *Plant Cell Environ.*, 18, 765–772, 1995.
- 485 [Sack, L., Scoffoni C., et al.: How do leaf veins influence the worldwide leaf economic spectrum? Review and synthesis. *Journal of Experimental Botany*, 64: 4053-4080, 2013.](#)
- [Sela, G.: Fertilization and irrigation: theory and best practices. Independently Published. SBN-13 979-8793313865, 2021.](#)
- Smith, N.G., and Dukes, J.S.: Drivers of leaf carbon exchange capacity across biomes at the continental scale. *Ecology*, 99, 1610–1620, 2018.
- 490 Smith, N., Smith, G., Keenan, T.F., Prentice, I.C., Wang, H., et al.: Global photosynthetic capacity is optimized to the environment. *Ecological Letters*, 22: 506–517. doi: 10.1111/ele.13210, 2019.
- Smith, N., Smith, G., Keenan, T.F., Prentice, I.C., Wang, H., et al.: R code of an ecosystem optimality theory for calculating the global distribution of leaf photosynthetic capacity. https://github.com/SmithEcophysLab/optimal_vcmax_R, 2022.
- 495 [Song X., Zhou, G., He, Q., and Zhou, H.: Quantitative response of maize Vcmax25 to persistent drought stress at different growth stages. *Water*, 13, <https://doi.org/10.3390/w13141971>, 2021.](#)

- Sun, Y., Frankenberg, C., Wood, J. D., Schimel, D. S., Jung, M., Guanter, L., et al.: OCO-2 advances photosynthesis observation from space via solar-induced chlorophyll fluorescence. *Science*, 358(6360), eaam5747, 2017.
- Verhoef, W.: Light scattering by leaf layers with application to canopy reflectance modeling: The SAIL model. *Remote Sensing of Environment*, 16, 125-141, 1984.
- 500 Wang, H., Prentice, I.C., Keenan, T.F., Davis, T.W., Wright, I.J., Cornwell, W.K. et al.: Towards a universal model for carbon dioxide uptake by plants. *Nat. Plants*, 3, 734–741, 2017.
- Wang, X., Chen, J. M., and Ju, W.: Photochemical Reflectance Index (PRI) can be used to improve the relationship between gross primary productivity (GPP) and sun-induced chlorophyll fluorescence (SIF). *Remote Sensing of Environment*, 246, 111888, 2020.
- 505 Walker, A. P., Quaipe, T., van Bodegom, P. M., De Kauwe, M. G., Keenan, T. F., Joiner, J., ... Woodward, F. I.: The impact of alternative trait-scaling hypotheses for the maximum photosynthetic carboxylation rate (V_{cmax}) on global gross primary production. *New Phytologist*, 215(4), 1370–1386, 2017.
- [Wright, I. J., Reich, P. B. et al.: The worldwide leaf economics spectrum. *Nature*, 428, 821-827, 2004.](#)
- Zhang, Y., Chen, J.M., Miller, J. and Noland, T.: Needle chlorophyll content retrieval from airborne hyperspectral imagery. *Remote Sensing of Environment*, 112: 3234-3247, 2008.
- 510 Xu, C., Fisher, R., Wullschleger, S. D., Wilson, C. J., Cai, M., and McDowell, N. G.: Toward a mechanistic modeling of nitrogen limitation on vegetation dynamics. *PLoS ONE*, 7(5), 1–11, 2012.

515

520

525

Table 1. Correlations by plant function type between V_{cmax} at growing season mean temperature (T_g) in four products (GOME-2 SIF, TROPOMI SIF, LCC and EOT) and a ground database with 3672 individual data points aggregated to 180 grids of 0.5° resolution.

Product	r^2 , p and RMSE ($\mu\text{ mol m}^{-2}\text{s}^{-1}$)	ENF, DNF, DBF (n=44)	EBF (n=58)	GRS (n=40)	CRP (n=39)	SHR (n=6)	ALL (n=187)
GOME-2	r^2	0.15	0.35	0.83	0.27	0.32	0.69
	RMSE	8.26	15.73	17.37	11.41	13.58	13.80
	p	<0.01	<0.001	<0.001	<0.001	0.25	<0.001
TROPOMI	r^2	0.31	0.66	0.85	0.65	0.90	0.80
	RMSE	5.57	9.55	13.32	5.50	5.55	8.99
	p	<0.001	<0.001	<0.001	<0.001	<0.01	<0.001
LCC	r^2	0.01	0.18	0.77	0.30	0.76	0.55
	RMSE	8.4	25.47	21.06	9.14	11.35	18.28
	p	0.54	<0.001	<0.001	<0.001	<0.05	<0.001
EOT	r^2	0.10	0.34	0.85	0.38	0.22	0.66
	RMSE	7.70	19.57	11.78	7.42	12.42	13.37
	p	0.042	<0.001	<0.001	<0.001	0.35	0.001

535

540

Table 2 Mean and standard deviation (SD) of V_{cmax} at the growing temperature ($V_{\text{cmax}T_g}$) and normalized to 25 °C ($V_{\text{cmax}25}$) for different plant functional types (PTF) calculated from the TROPOMI and ecological optimality theory (EOT) products in comparison with two ground-based databases (Smith et al., 2019 and Kattge et al., 2009).

545

		TROPOMI		EOT		Smith 2019		Kattge 2009	
PFT	($\mu\text{mol m}^{-2}\text{s}^{-1}$)	Mean	SD	Mean	SD	Mean	SD	Mean	SD
ENF	$V_{\text{cmax}25}$	32.36	12.51	60.66	7.19	53.70	26.95	62.50	24.70
	V_{cmaxTg}	7.31	3.62	13.68	2.97	17.43	11.13		550
EBF	$V_{\text{cmax}25}$	46.89	13.02	54.55	6.79	45.83	23.27	43.80	16.83
	V_{cmaxTg}	44.22	15.98	50.88	12.19	37.12	23.59		
DNF	$V_{\text{cmax}25}$	44.38	8.93	60.50	5.05	44.82	23.34	39.10	11.70
	V_{cmaxTg}	10.95	2.58	14.93	2.09	11.59	6.28		
DBF	$V_{\text{cmax}25}$	44.42	16.42	59.60	6.31	51.31	25.06	57.70	21.20
	V_{cmaxTg}	18.12	17.07	22.68	15.68	24.31	20.72		555
SHR	$V_{\text{cmax}25}$	53.30	13.60	61.37	7.55	50.63	27.75	57.85	19.55
	V_{cmaxTg}	13.21	11.24	15.76	14.54	31.88	27.80		
GRS	$V_{\text{cmax}25}$	74.74	22.76	69.45	12.37	82.70	47.86	78.20	31.10
	V_{cmaxTg}	49.30	40.10	41.42	27.85	21.65	18.25		560
CRP	$V_{\text{cmax}25}$	87.57	17.42	62.12	9.59	90.21	32.13	100.70	36.60
	V_{cmaxTg}	54.83	37.14	39.63	26.72	42.11	22.64		

565

570

575

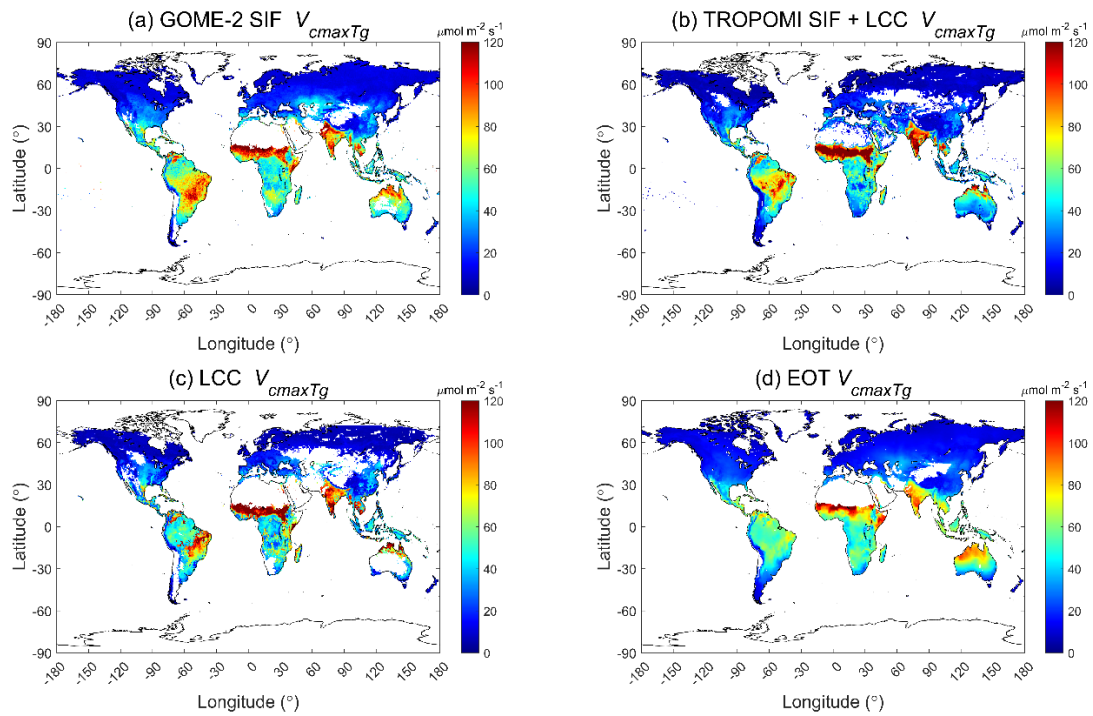
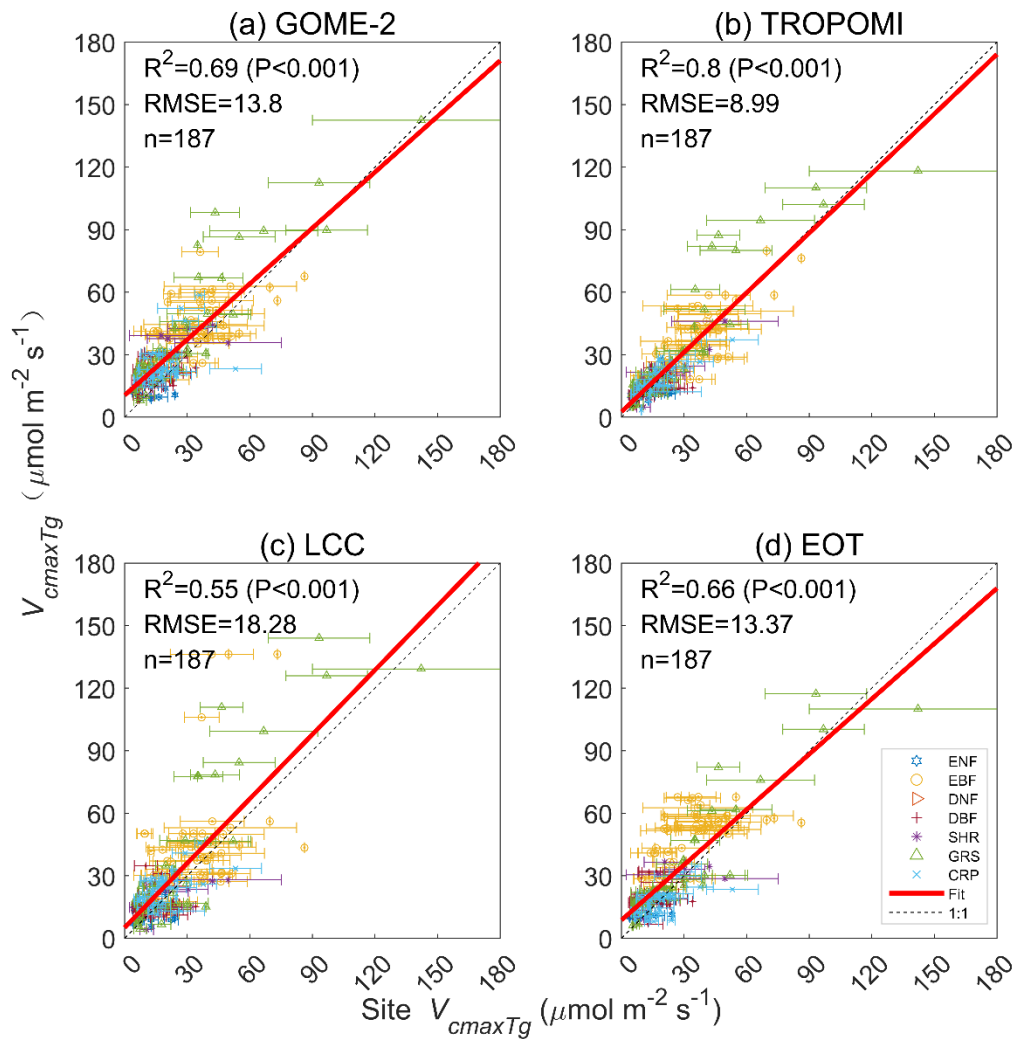
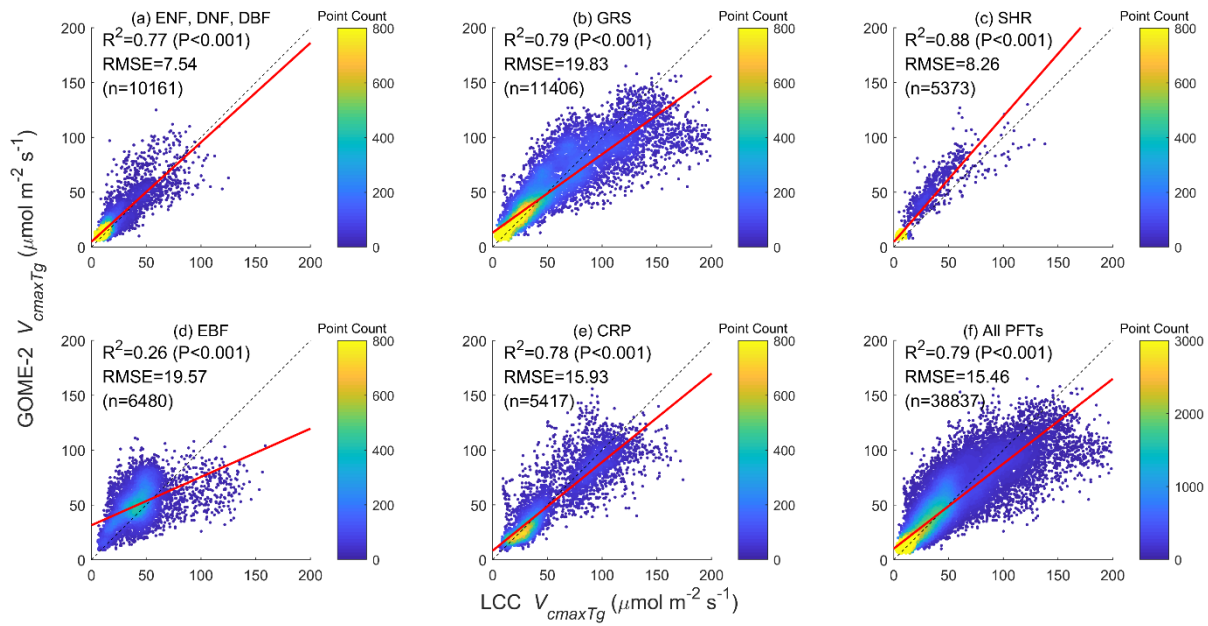


Figure 1. Global distributions of V_{cmaxTg} at the mean growing season temperature derived using (a) GOME-2 SIF (2007-2011), (b) TROPOMI SIF+LCC (2018) constrained by leaf chlorophyll content (LCC), (c) LCC (2017), and (d) ecological optimality theory (1901-2015). White areas are missing data



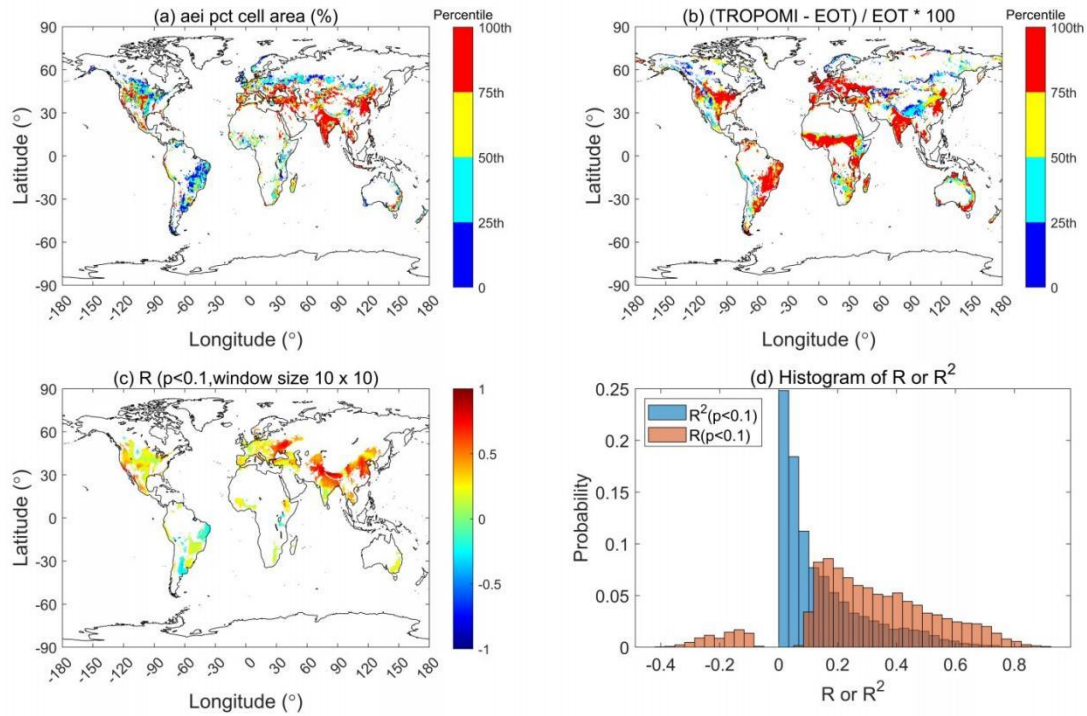
580 **Figure 2. Comparisons of V_{cmax} at growing season mean temperature (T_g) derived from GOME-2 SIF, TROPOMI SIF+LCC, LCC and optimality theory (EOT) against a ground database with 3672 individual data points aggregated to 180 grids of 0.5° resolution. The root mean square error (RMSE) is in unit of $\mu\text{mol m}^{-2}\text{s}^{-1}$.**



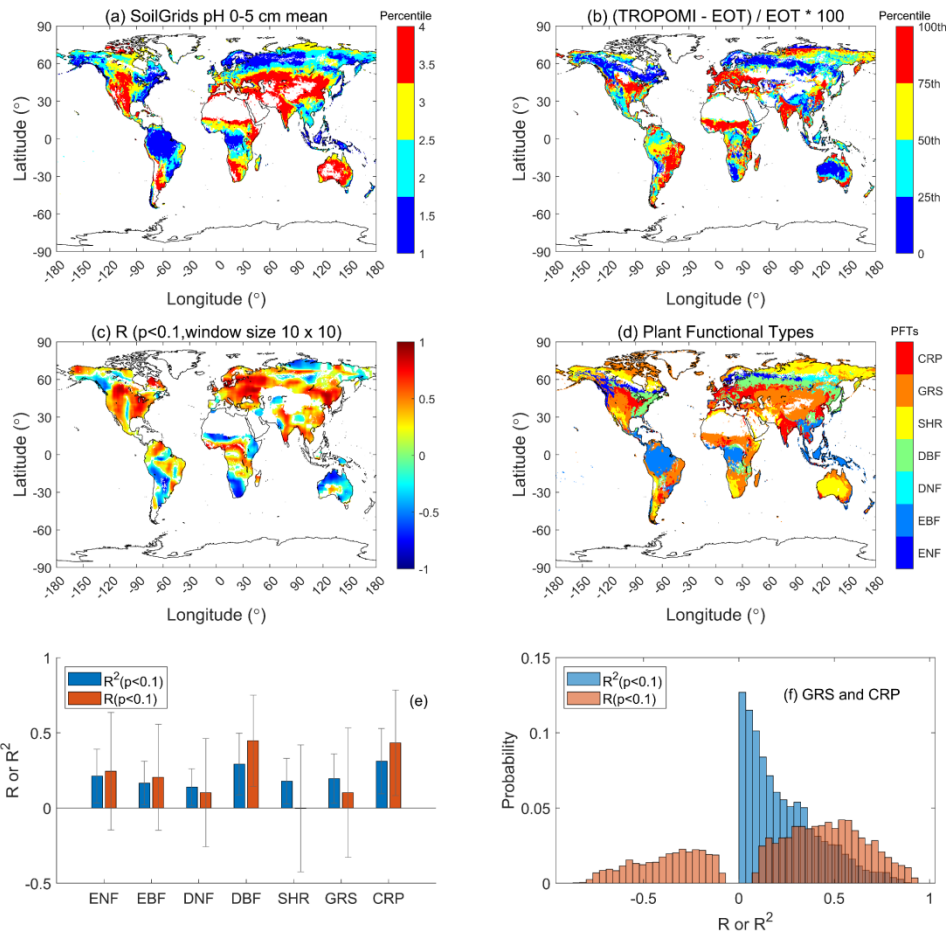
585

Figure 3. Comparisons of SIF-derived and LCC-derived V_{cmax} values for a group of three PFTs and four individual PFTs as well as all PFTs combined. These two sets of V_{cmax} derived independently using two different remote sensing techniques are very well correlated for all PFTs except for the evergreen broadleaf forests (EBF) in tropical areas where frequent clouds degrade the quality of both SIF and LCC datasets.

590



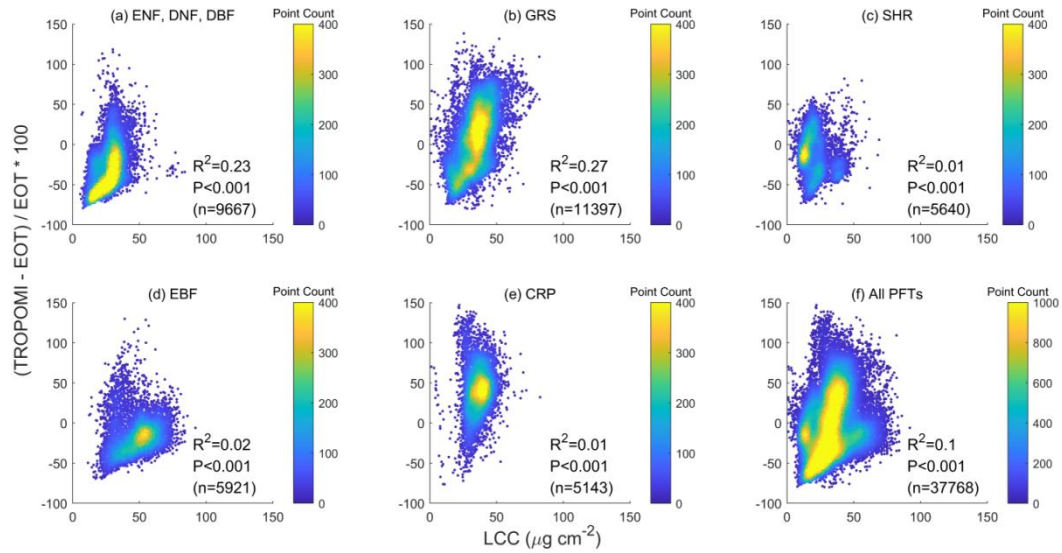
595 **Figure 4. The influence of irrigation on V_{cmax} over cropland and grassland, detected by TROPOMI SIF+LCC at 0.5° resolution, where (a) is the actual area irrigated in percent of cell area (aai pct cell area) in recent decades, (b) the relative difference in V_{cmax} (ΔV_{cmax}) between TROPOMI and ecological optimality theory (EOT), i.e. $\Delta V_{cmax} = (TROPOMI - EOT) / EOT$, (c) the correlation coefficient (R) between actual irrigated area percentage and ΔV_{cmax} within sliding windows of 10×10 pixels, and (d) the histograms of R and R^2 values in (c) for cropland and grassland. ΔV_{cmax} is significantly correlated with percent area irrigated in both cropland (R=0.26, $p < 0.001$) and grassland (R=0.11, $p < 0.001$) at the global scale.**



600

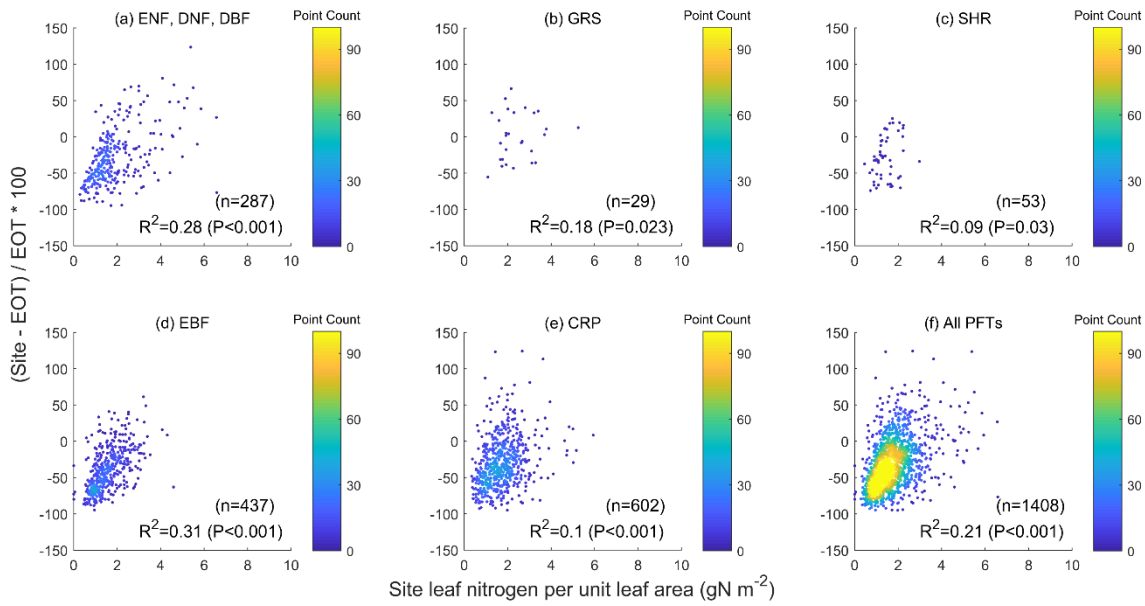
Figure 5. Soil pH has significant influence on V_{cmax} detected by TROPOMI SIF+LCC at 0.5° resolution. (a) soil pH in the top 0-5 cm layer, (b) relative difference in V_{cmax} (ΔV_{cmax}) between TROPOMI and ecological optimality theory (EOT), i.e. $\Delta V_{cmax} = (\text{TROPOMI} - \text{EOT}) / \text{EOT}$, (c) correlation coefficient (R) between soil pH and ΔV_{cmax} within sliding windows of 10 x 10 pixels, (d) PTF distribution, (e) summary of mean correlation coefficient R and R^2 values in (c) by PFTs, and (f) histograms of R and R^2 values in (c) for grassland (GRS) and cropland (CRP). In 43% of GRS and CRP pixels, ΔV_{cmax} is positively and significantly ($p < 0.1$) correlated with soil pH.

605



610 **Figure 6.** The relative difference in V_{cmaxTg} (ΔV_{cmax}) between TROPOMI and ecological optimality theory (EOT), i.e. $\Delta V_{cmax}=(TROPOMI-EOT)/EOT$, is significantly correlated to leaf chlorophyll content (LCC) as a proxy of the leaf nutrient condition. All PFTs are included. The correlation is statistically highly significant with $p<0.001$ for individual PFTs and for all PFTs combined.

615



620 **Figure 7. Influence of leaf nitrogen content on the relative difference between V_{maxTg} values measured at ground sites and derived from an ecological optimality theory (EOT) using the available database (Smith et al., 2019). The influence is highly significant for all plant functional types (i.e. $p < 0.001$). The slopes of the regressions of the relative difference in V_{max} against LCC or ground leaf nitrogen data are similar, in agreement with the global modeling results that levels of nutrient limitation to plant growth are similar among different PFTs (Fisher et al., 2012).**

625

630

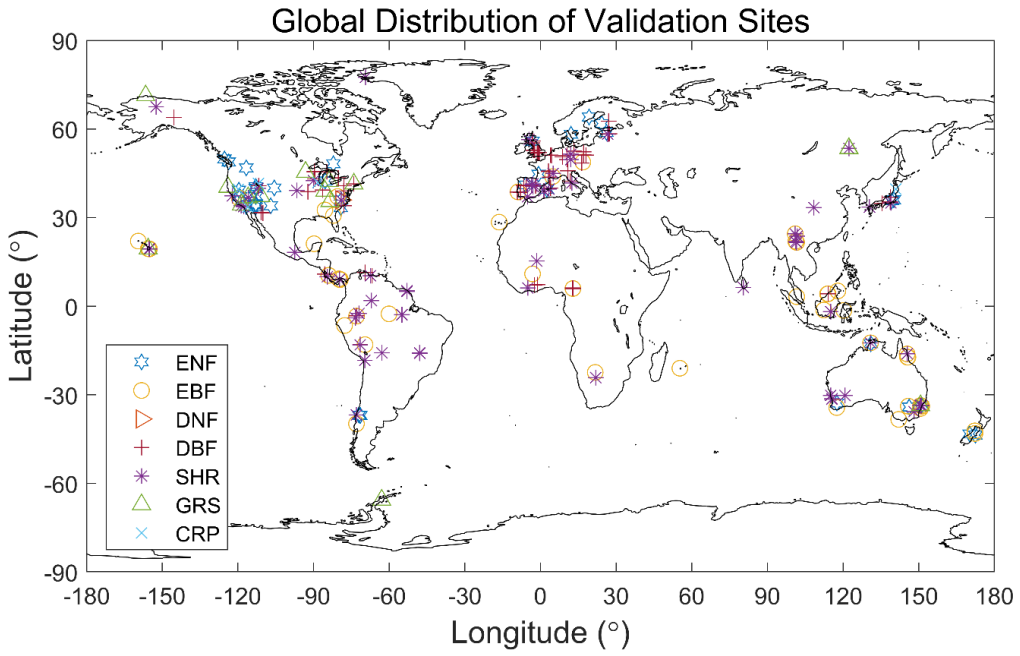
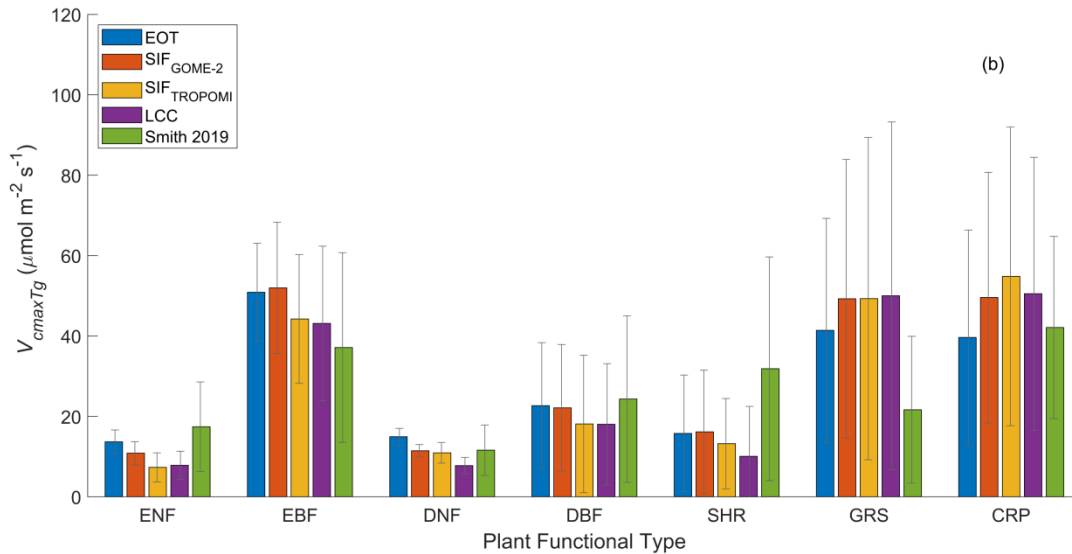
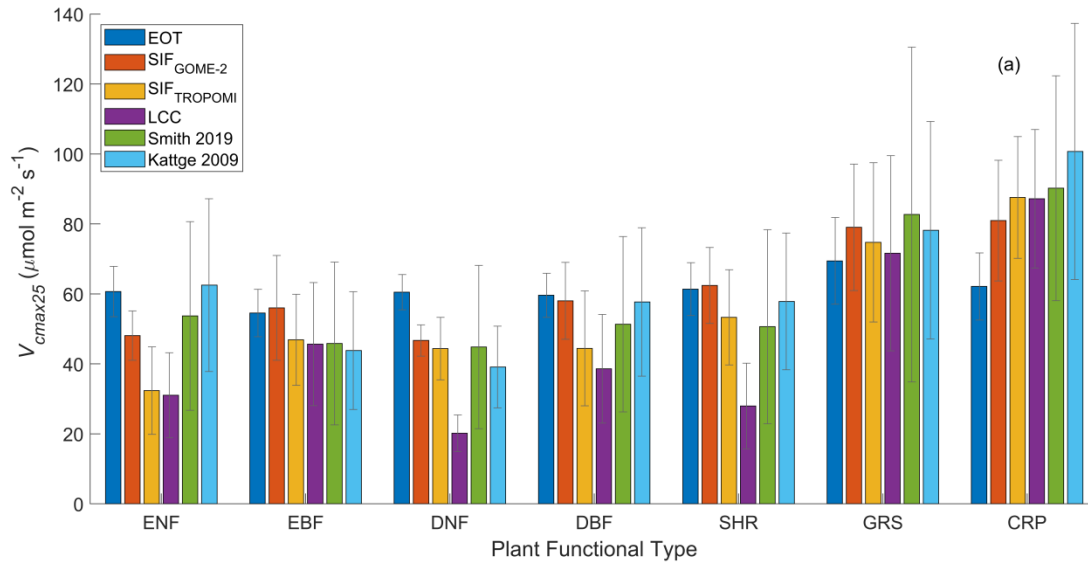


Figure 8. Distribution of ground sites of the database of Smith et al. (2019) after aggregation to 0.5 grids for the different plant functional types.

635



640 **Figure 9.** Mean and standard deviation of V_{cmaxTg} at growth temperature and V_{cmax25} (normalized to 25 °C) derived from
 | GOME-2 SIF, TROPOMI SIF+LCC, LCC and ecological optimality theory (EOT) in comparison with two ground databases
 (Smith 2019 and Kattge 2009) for the main PFTs at growth temperature. Kattge 2009 contains more V_{cmax25} than V_{cmaxTg} so only
 V_{cmax25} is included in (a). The EOT product has considerably smaller V_{cmaxTg} in grassland (GRS) and crops (CRP) than the three
 645 remote sensing products. All four products have considerably higher V_{cmaxTg} than the ground site measurements in grassland
 mostly because the number of site measurements are too small to be representative of the global average. After the temperature
 normalization, the differences among the products become much smaller.

Code/Data Availability

650 The V_{cmax} datasets presented in this paper are available at <https://doi.org/10.5281/zenodo.6466968> (Chen et al., 2022). It includes the following three global 0.5 degree V_{cmax} datasets at growth temperature:

1) V_{cmax} from GOME-2 SIF: GOME2_Vcmax_Tg_05deg.tif

2) V_{cmax} from TROPOMI SIF+LCC: TROPOMI_Vmax_Tg_mean.mat

3) V_{cmax} from global leaf chlorophyll content map (Croft et al., 2020, RSE): LCC_Vcmax_Tg_mean.mat

655 The geographic reference are the same for all three datasets, conforming to that in the geotiff file.

Any questions on the dataset, please contact: Dr. Jing M. Chen, jing.chen@utoronto.ca.

The functions written in R for calculating V_{cmax} using the ecological optimality theory are available at https://github.com/SmithEcophysLab/optimal_vcmax_R (Smith et al., 2022).

660

Author Contribution

Conceptualization: JMC, TFK, ICP

Data curation: RW, YL, HC, NGS

Formal analysis: JMC, RW, YL

665 Funding acquisition: JMC, NS, TK, CP

Investigation: JMC, RW, YL

Methodology: YL, LH, HC, XL, HW

Software: RW, LH, YL

Supervision: JMC

670 Validation: RW, NGS, TK

Visualization: RW, YL

Writing—original draft: JMC

Writing—review & editing: HC, RW, NGS, TK, ICP, HW, WJ, YZ, ND

675 Competing Interests

The authors declare that they have no conflict of interest.

Right to reproduce any materials

Not applicable